第 29 卷第 8 期 无 机 化 学 学 报 Vol.29 No.8
2013 年 8 月 CHINESE JOURNAL OF INORGANIC CHEMISTRY 1759-1768

基于铜基底的 TiO_2 纳米管阵列储锂性能

陈公德 张卫新* 杨则恒 王 强 姚宏旭
(合肥工业大学化工学院,可控化学与材料化工安徽省重点实验室,合肥 230009)

摘要: 研究了基于铜基底的 TiO_2 纳米管阵列直接作为锂离子电池电极的储锂性能。以铜基底上生长的 $Cu(OH)_2$ 纳米棒阵列为模板,采用自牺牲模板法,通过外向包覆与内向刻蚀,制备了非晶态的 TiO_2 纳米管阵列,然后将其在 500 ℃下退火处理 4 h,获得锐钛矿型 TiO_2 纳米管阵列。采用 X 射线衍射、场发射扫描电镜、透射电镜、热重分析对样品进行表征;采用恒电流充放电、循环伏安和交流阻抗谱测试对退火前后 TiO_2 纳米管阵列的电化学性能进行研究。结果表明:与非晶态的 TiO_2 纳米管阵列相比,锐钛矿型 TiO_2 纳米管阵列吸附水的含量低,结晶度高,电荷迁移阻力小,锂离子扩散系数大,结构稳定,具有更好的循环性能和倍率性能;在 0.2C 下,其首次放电比容量为 353 $mAh\cdot g^{-1}$,经过 40 次循环后的放电比容量仍为 243 $mAh\cdot g^{-1}$,在 8C 下的放电比容量为 90 $mAh\cdot g^{-1}$。

关键词: TiO_2; 纳米管阵列; 模板; 负极; 锂离子电池
中图分类号: O614.33; TM 912.9 **文献标识码**: A **文章编号**: 10014861(2013)08-1759-10
DOI:10.3969/j.issn.1001-4861.2013.00.308

Lithium Storage Performances of TiO_2 Nanotube Arrays on Copper Substrate

CHEN Gong-De ZHANG Wei-Xin* YANG Ze-Heng WANG Qiang YAO Hong-Xu
(*School of Chemical Engineering, Hefei University of Technology, Anhui Key Laboratory of Controllable Chemistry Reaction & Material Chemical Engineering, Hefei* 230009, *China*)

Abstract: Lithium storage performances of TiO_2 nanotube arrays on copper substrate as electrodes in lithium-ion batteries were investigated. Amorphous TiO_2 nanotube arrays were prepared via a sacrificial template method from outward coating of TiO_2 and inward etching of $Cu(OH)_2$ nanorod array templates on copper substrate. Anatase TiO_2 nanotube arrays were obtained by post-heating the sample at 500 ℃ for 4 h. The samples were characterized by X-ray diffraction (XRD), field-emission scanning electron microscopy (FESEM), transmission electron microscopy (TEM), and thermogravimetric analysis (TGA). The electrochemical performances of amorphous and anatase TiO_2 nanotube arrays were investigated by galvanostatic charge-discharge measurements, cyclic voltammetry (CV), and electrochemical impedance spectroscopy (EIS). The results indicate that compared with amorphous TiO_2 nanotube arrays, anatase TiO_2 nanotube arrays exhibit a superior rate capability and cycling performance due to their lower amounts of adsorbed water, higher crystallization, lower charge-transfer resistance, higher lithium-ion diffusion coefficient, and more stable one-dimensional tubular structure. They show an initial specific discharge capacity of 353 $mAh\cdot g^{-1}$ and 243 $mAh\cdot g^{-1}$ even after 40 cycles at 0.2C. At a high rate of 8C, their discharge capacity can reach 90 $mAh\cdot g^{-1}$.

Key words: TiO_2; nanotube arrays; templates; anode; lithium-ion batteries

收稿日期:2013-02-26。收修改稿日期:2013-06-10。
国家自然科学基金(No.21271058, 21176054, 20871038),安徽省教育厅创新团队项目(TD200702)资助项目。
*通讯联系人。E-mail:wxzhang@hfut.edu.cn

As one of the most promising and viable green options for energy storage, rechargeable lithium-ion batteries have attracted considerable attention over past decades. Graphite is commonly used as the anode material for lithium-ion batteries. However, graphite-based materials suffer from several disadvantages including low lithium intercalation voltage, limited capacity, and poor rate performance. All these problems lead to concern for safety and loss of capacity and stimulate researchers to explore novel alternative anode materials.

TiO_2 is a promising candidate for anode due to its high Li-insertion potential (1.5~1.8 V versus Li^+/Li), small volume expansion ratio (3%)[1] during the process of Li-insertion/ extraction, good cycling performance, chemical stability, low cost, and minimal toxicity. In 1992, Macklin and Neat [2] first reported the high capacity and reversibility of lithium insertion into titanium oxide electrodes in lithium batteries. Since that, much attention has been paid to understanding and optimizing TiO_2 anode.

However, bulk TiO_2 materials show unsatisfactory electrochemical performances due to sluggish kinetics of lithium ion intercalation and electron transfer. Recently, nanostructured TiO_2 materials designed as the electrodes for Li-ion batteries have drawn much attention. They can reside the active sites close to the surface, effectively shorten the diffusion path for lithium ions and then increase the charge-transfer rates, which are helpful to enhance their electrochemical performances. TiO_2 nanostructured materials with various morphologies have been prepared as potential anode materials for lithium-ion batteries, such as nanosheets [3], nanorods [4], nanotubes [5], hierarchical spheres assembled from nanosheets[6], and so forth.

Among them, TiO_2 nanotube arrays grown directly on a current-collecting substrate as electrodes in lithium-ion batteries have been paid much attention given that they have higher surface-to-volume ratio, much better electron transportation capability, easy diffusion of electrolyte into the inner region of the electrode, and relatively lower volume variation during the charge-discharge process in comparison with the bulk counterparts [7-8]. Currently, TiO_2 nanotube arrays have been prepared by various methods, including electrochemical titanium anodization method[9-10], anodic aluminum oxide (AAO) template method [11-12], seeded growth method [13]. However, to the best of our knowledge, there have been only several studies involving the lithium storage performance of the TiO_2 nanotube arrays. Ortiz and coworkers [14] prepared TiO_2 nanotube arrays by an anodization method and reported that amorphous TiO_2 nanotube arrays had an larger irreversible capacity due to larger amounts of adsorbed water, defects and bigger discharge capacity, and anatase TiO_2 nanotube arrays exhibited a higher cycling efficiency due to the smaller amount of structural defects and Li ion traps. Fang et al [15] reported that amorphous TiO_2 nanotube array electrode had a higher rate capability in comparison with anatase TiO_2 nanotube arrays because of the former′s higher Li-diffusion coefficient and lower electronic conductivity.

In this work, lithium storage performances of amorphous and anatase TiO_2 nanotube arrays on copper substrate as electrodes in lithium-ion batteries have been respectively investigated. We have reported free-standing TiO_2 nanotube arrays on copper substrate fabricated via a sacrificial template method[16]. The as-prepared TiO_2 nanotube arrays have electrical contact directly with the substrate and eliminate the needs for binders and conducting additives. EIS, TGA, and morphological changes after 100 discharge-charge cycles of the two samples have been compared in order to reveal the enhanced electrochemical performances of anatase TiO_2 nanotube arrays.

1 Experimental

1.1 Preparation of $Cu(OH)_2$ nanorod array templates

All chemicals, purchased from Sinopharm Chemical Reagent Co., Ltd, China, were used as-received without further purification.

The procedure for synthesizing $Cu(OH)_2$ nanorod arrays grown on copper foil were reported in our previous papers [17-18]. Typically, a piece of copper foil ($10\times10\times0.25$ mm^3, 99.99%) was ultrasonically cleaned

in acetone, absolute ethanol, and distilled water in turn, and dried in air before use. Then it was immersed in an aqueous solution containing 10 mL of distilled water, 2 mL of NaOH solution (10 mol·L^{-1}), 1 mL of $(NH_4)_2S_2O_8$ solution (1 mol·L^{-1}), and 1.0 mL of ammonia solution (25wt%). After 50 min of reaction at room temperature, the copper foil with a blue film on the surface was taken out, rinsed with distilled water and absolute ethanol, and dried in air.

1.2 Preparation of TiO_2 nanotube arrays

The details for synthesizing TiO_2 nanotube arrays were described in our previous study[16]. First, $Cu(OH)_2$ nanorod arrays were immersed in a uniform solution containing 1 mL of Ti $(OC_4H_9)_4$ and 5 mL of ethanol. After 10 min, the sample was taken out and placed in air for an hour. Then, the obtained sample was immersed in a 10 mL of ammonia aqueous solution (12.5wt%). After 16 h, the sample was taken out, rinsed with distilled water and ethanol, and dried in air. Finally, the sample was annealed in a nitrogen atmosphere at 500 ℃ for 4 h.

1.3 Characterization of the samples

X-ray diffraction (XRD) patterns of samples were recorded on a Rigaku D/max-rB X-ray diffractometer with a Cu $K\alpha$ radiation source (λ =0.154 178 nm) operated at 40 kV and 80 mA. The step width was 0.02 degrees. The morphologies and structures of the samples were characterized using field-emission scanning electron microscope (FESEM) (FEI Sirion-200), and transmission electron microscope (TEM) (Hitachi H-800), respectively. The TEM measurement was performed at an accelerating voltage of 200 kV. Thermogravimetric analysis (TGA) was conducted on TGA Q5000 thermal analyzer; the samples were heated from room temperature to 700 ℃ at a rate of 5 ℃·min^{-1} in a steady flow of dry N_2 (75 mL·min^{-1}).

1.4 Electrode preparation and electrochemical measurements

TiO_2 nanotube arrays film on copper substrate with a diameter of 11 mm were dried in the vacuum oven at 60 ℃ for 4 h. The net mass of active materials was measured by a microbalance (SHIMADZU AUW220D, a precision of 0.01 mg). Test cells were assembled into two-electrode coin-type cells with a Li metal counter electrode, a separator (Celgard 2400), and an electrolyte of 1 mol·L^{-1} $LiPF_6$ in a 1∶1 (volume) mixture of ethylene carbonate and dimethyl carbonate. Cell assembly was carried out in an argon-filled glove box. The galvanostatic charge-discharge tests were performed on a battery testing system (BTS-5V/10 mA, Neware Technology Limited Corporation, China) with cutoff voltages between 3.0 and 1.0 V (versus Li^+/Li) at different rates from 0.1C to 8C (1C=300 mAh·g^{-1}). Cyclic voltammetry (CV) was recorded at a scan rate of 0.1 mV·s^{-1} from 3.0 to 1.0 V (versus Li^+/Li) on an electrochemical workstation (CHI-660B, Shanghai Chenhua Instrument Limited Corporation, China). Electrochemical impedance spectroscopy (EIS) results of the samples were measured with the excitation potential of 5 mV and the frequency range from 100 kHz to 10 mHz.

2 Results and discussion

2.1 Results

2.1.1 Material characterization

The composition and phase purity of as-prepared samples were characterized by XRD patterns (Fig.1). As shown in Fig.1a, the diffraction peaks marked with "*" come from the copper substrate. No characteristic peaks of TiO_2 can be observed, which indicates that TiO_2 nanotube arrays without post-heating are amorphous. Thermal treatment of the sample in a nitrogen atmosphere at 500 ℃ for 4 h leads to the formation of

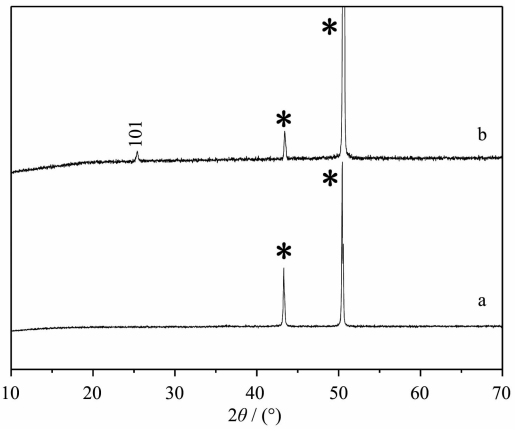

Fig.1 XRD patterns of TiO_2 nanotube arrays on copper substrates (a) without post-heating and (b) annealed at 500 ℃ for 4 h

anatase phase. A characteristic peak located at 25.3° can be indexed to the (101) plane of the anatase TiO_2 (PDF 21-1272). Since the film mass is only 0.14 mg·cm^{-2}, the peak intensity of the anatase TiO_2 is low.

Fig.2 shows the FESEM and TEM images of amorphous and anatase TiO_2 nanotube arrays. As observed in Fig.2a, amorphous TiO_2 nanotube arrays are free-standing and well-ordered. Some broken structures can be found in Fig.2b, which demonstrates the tubular structure of the prepared samples. TiO_2 nanotubes have lengths of 10~15 μm and diameters of around 500 nm. After heat treatment, structures of nanoarrays are still well-retained, which can be observed in Fig.1c. The TEM results of anatase TiO_2 nanotubes in Fig.2d shows the obvious contrast between the exterior (dark) and interior (pale), indicating that the hollow nanostructure of the annealed samples.

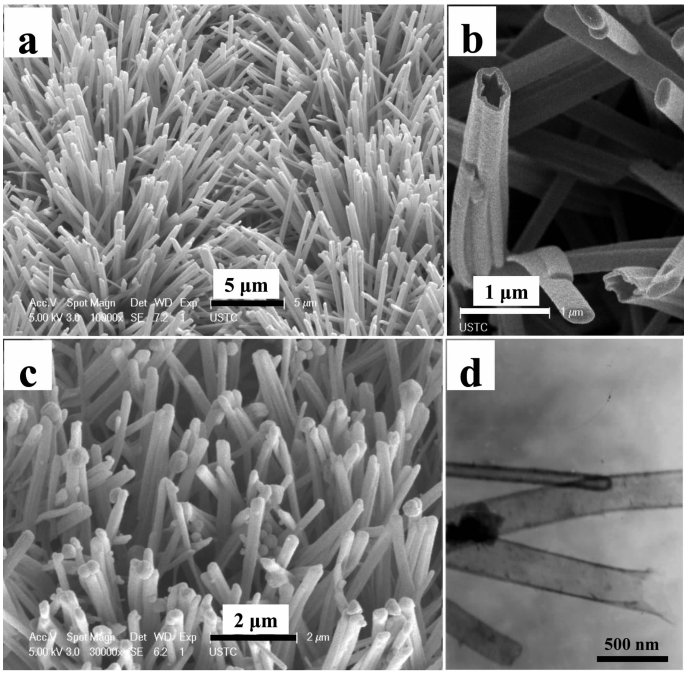

Fig.2 (a, b) FESEM images of amorphous TiO_2 nanotube arrays; (c) FESEM and (d) TEM images of anatase TiO_2 nanotube arrays

2.1.2 Electrochemical performances

Fig.3a and b display the first ten discharge-charge curves of the samples at 0.2C. As clearly shown in Fig. 3a, anatase TiO_2 nanotube array electrode exhibits two voltage plateaus, appearing at 1.76 V and 1.91 V during the discharge (Li ion insertion) and charge (Li ion extraction) process, respectively, which is consistent with the electrochemical characteristics of anatase TiO_2

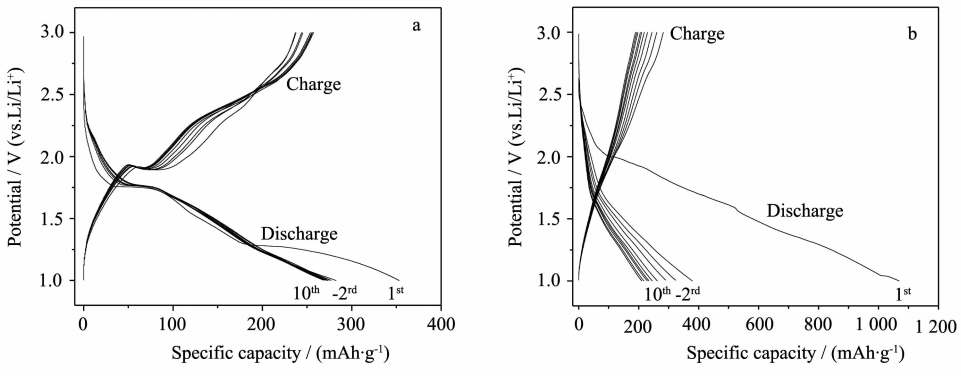

Fig.3 Initial ten discharge-charge curves of (a) anatase TiO_2 nanotube arrays and (b) amorphous TiO_2 nanotube arrays at 0.2C

reported in the previous literature [19]. A total discharge capacity of 353 mAh·g^{-1} is obtained in the first cycle, including a reversible capacity of 283 mAh·g^{-1} in the second discharge. The corresponding irreversible capacity is 70 mAh·g^{-1}. The initial capacity loss of 19.8% is much lower than that of reported anatase TiO_2 electrodes such as TiO_2 hollow spheres [20]. Though the columbic efficiency for the first cycle is only 67.1%, it increases dramatically in the following cycles. After 10 cycles, the discharge capacity is 271 mAh·g^{-1}, indicating their good capacity retention. As for amorphous TiO_2 nanotube arrays, no plateau is observed during the discharge and charge process (Fig.3b). The discharge capacity of the first and second cycle is 1069 and 379 mAh·g^{-1}, respectively. The corresponding capacity fading is 690 mAh·g^{-1}, which is much larger than that of crystallized TiO_2 electrode [14]. After 10 cycles, the discharge capacity is 217 mAh·g^{-1}.

To investigate the rate capability of the prepared electrodes, they were discharged at different current rates, and the results are displayed in Fig.4. Despite the obvious capacity fading of amorphous TiO_2 nanotube arrays at 0.1C, a relatively stable cycling performance is exhibited for both samples at different rates. The anatase and amorphous TiO_2 nanotube electrodes present discharge capacities of 346 and 512 mAh·g^{-1} at 0.1 C, and then drop to 275 and 238 mAh·g^{-1}, 224 and 138 mAh·g^{-1}, 185 and 88 mAh·g^{-1}, 155 and 50 mAh·g^{-1} at 0.2C, 0.5C, 1C, and 2C, respectively. It is clear that anatase TiO_2 nanotube arrays deliver larger discharge capacities than amorphous TiO_2 nanotube arrays at discharge rates from 0.2C to 2C. When the rate increases to 4C and 8C, anatase TiO_2 nanotube arrays show discharge capacities of 127 and 90 mAh·g^{-1}, respectively, while amorphous TiO_2 nanotube arrays of 19 and 13 mAh·g^{-1}, demonstrating a superior rate performance of the crystallized anatase electrode.

A more visible comparison is presented in inset of Fig.4. Apparently, the discharge capacity retention of the two samples decreases with the elevation of discharge rates. However, anatase TiO_2 nanotube arrays presents a slower decay of capacity retention rate in comparison with amorphous TiO_2 nanotube arrays,

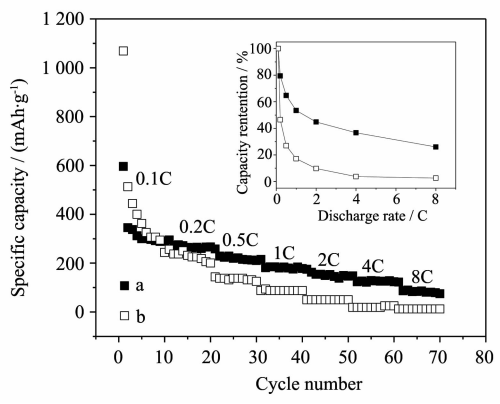

The capacities of each rate were extracted from the second cycle

Fig.4　Cycling performances of (a) anatase TiO_2 nanotube arrays and (b) amorphous TiO_2 nanotube arrays at various current rates. (Inset: discharge capacity retention depending on discharge rates)

indicating that thermal treatment is beneficial to improve the rate capability of the samples.

Fig.5 shows the cycling performances of anatase and amorphous TiO_2 nanotube arrays at 0.2C and 1C, respectively. As observed, anatase TiO_2 array electrode suffers the major fading of discharge capacity in the first two cycles. At a low discharge rate of 0.2C, the discharge capacity decreases from 353 to 283 mAh·g^{-1}. After 40 cycles, the discharge capacity can reach 243 mAh·g^{-1}, and the average capacity loss per cycle from 2nd to 40th cycle is only 1.0 mAh·g^{-1}, manifesting a good capacity retention rate (85.6%) from 2nd to 40th cycle. As for amorphous TiO_2 nanotube arrays, the obvious decay of discharge capacity also appears in the initial two

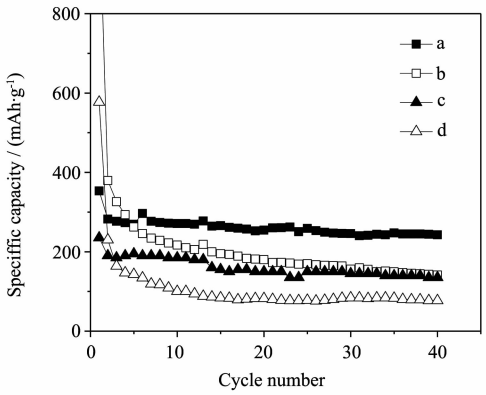

Fig.5　Cycling performances of anatase TiO_2 nanotube arrays (solid symbols) and amorphous TiO_2 nanotube arrays (open symbols) at current rates of (a, b) 0.2C and (c, d) 1C

cycles, from 1 069 to 379 mAh·g^{-1}. The reversible capacity decreases gradually in the subsequent cycles. After 40 cycles, the discharge capacity of amorphous electrode is only 141 mAh·g^{-1}, and the cycling efficiency from 2nd to 40th is 37.2%. With the increase of the discharge rate from 0.2 to 1C the discharge capacity of both samples decreases. The cycling efficiency obtained from 2nd to 40th cycle is 71% and 33% for anatase TiO_2 nanotube arrays and amorphous TiO_2 nanotube arrays, respectively.

Fig.6 shows the representative cyclic voltammograms (CVs) of the samples. As observed from the CVs of anatase TiO_2 nanotube arrays in Fig.6a, two well-defined current peaks at 1.71~1.73 V and 1.98~2.00 V are in agreement with previous report[21] and also consistent with the plateaus in the discharge-charge curves of Fig.3a. The 0.25 V interval spacing between the cathodic and anodic peaks is much lower than the typical reported value (0.35~0.4 V) for nanocrystalline TiO_2 [4,6]. The peaks at about 1.73 V can be assigned to the transition from Li-poor phase to Li-rich phase. Notably, a peak at 1.17 V presents in the first catholic scan and disappears in the second cycle, which indicates an irreversible process and is consistent with the first two discharge curves of Fig.3a. Besides, the position and intensity of the peaks remain unchanged in the subsequent cycle, suggesting a good reversibility of the electrode material. The CVs of amorphous TiO_2 nanotube arrays are presented in Fig.6b. Because the sample does not have stable crystal structure for the intercalation and extraction of Li ions, there is no obvious peak observed. It is in accordance with the discharge-charge curves of amorphous TiO_2 nanotube arrays in Fig.3b. A large hump between 1.2 and 2.0 V presented in the first catholic scan disappears in the following cycles, suggesting a large irreversible process. This phenomenon is in agreement with the first two discharge curves of Fig.3b.

Fig.7a shows the Nyquist plots of anatase and amorphous TiO_2 nanotube arrays within the frequency

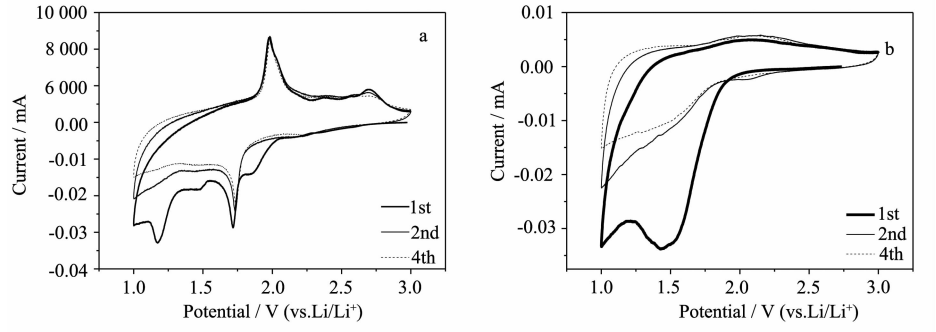

Fig.6 Representative cyclic voltammograms of (a) anatase TiO_2 nanotube arrays and (b) amorphous TiO_2 nanotube arrays at a scan rate of 0.1 mV·s^{-1} within the potential range of 3.0~1.0 V vs. Li/Li$^+$

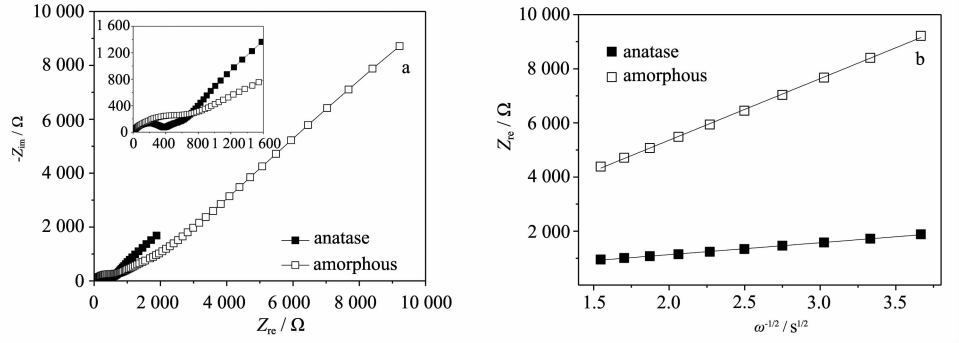

Fig.7 (a) Electrochemical impedance spectroscopy of TiO_2 nanotube arrays within the frequency range of 100 kHz to 10 mHz (The inset: magnified diagram) and (b) the relationship between Z_{re} and $\omega^{-1/2}$ at low frequency

range of 100 kHz to 10 mHz, respectively. Both EIS profiles show a semicircle in the high frequency region and a straight line in the low frequency region. The intercept impedance on the real axis represents the solution resistance (R_e). The numerical value of the diameter of the semicircle on the Z_{re} axis approximately equals the charge-transfer resistance (R_{ct}). The low frequency region of the straight line reflects the Warburg diffusion of the lithium ions in the bulk electrode material [22]. As shown in Fig.7a, the solution resistance of two samples is almost the same because the same electrolyte was used. Anatase TiO_2 nanotube arrays have a much smaller charge-transfer resistance (380 Ω) than amorphous TiO_2 nanotube arrays (690 Ω).

Fig.7b shows the relationship between Z_{re} and $\omega^{-1/2}$ (ω represents the angular frequency, s^{-1}) in the low frequency region. Based on the Eq.**1** [23], the Warburg coefficient σ_w of anatase and amorphous TiO_2 nanotube arrays is 440.88 and 2276.66 $\Omega \cdot s^{-1/2}$, respectively. In Eq.**2**[23], D ($cm^2 \cdot s^{-1}$) is lithium-ion diffusion coefficient, R is gas constant (8.314 $J \cdot mol^{-1} \cdot K^{-1}$), T is absolute temperature (298.15 K), A is the electrode area (0.95 cm^2), n is the mole number of electrons involved in the redox process (n =0.5) [24], C is the lithium-ion concentration in TiO_2 electrode (0.024 $mol \cdot cm^{-3}$)[24-26], and F is the Faraday constant (96 486 $C \cdot mol^{-1}$). According to Eq.**2** [23], the lithium -ion diffusion coefficient can be calculated to be 4.71×10^{-15} and 1.76×10^{-16} $cm^2 \cdot s^{-1}$, respectively. The value is consistent with the previously reported data of lithium-ion diffusion coefficient in anatase (10^{-13}~10^{-17} $cm^2 \cdot s^{-1}$) [25]. The result indicates that anatase TiO_2 nanotube arrays have a much

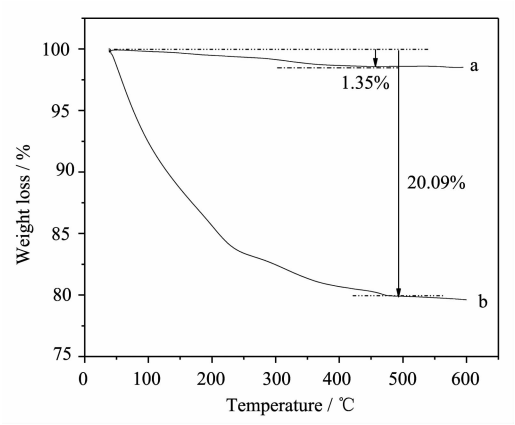

Fig.8　Thermogravimetric analysis curves of (a) anatase TiO_2 nanotubes and (b) amorphous TiO_2 nanotubes (all samples were scrapped from copper substrates)

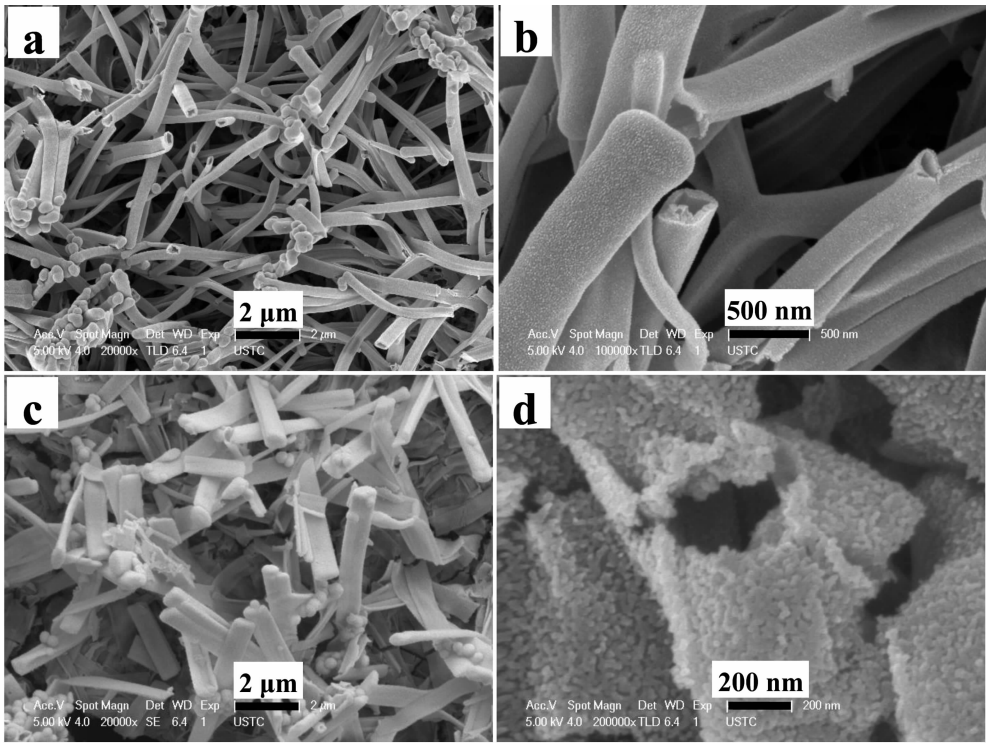

Fig.9　FESEM images of (a, b) anatase TiO_2 nanotube arrays and (c, d) amorphous TiO_2 nanotube arrays after 100 discharge-charge cycles at 0.2C

higher lithium-ion diffusion coefficient than amorphous TiO_2 nanotube arrays.

$$Z_{re} = R_e + R_{ct} + \sigma_w \omega^{-1/2} \quad (1)$$

$$D = R^2T^2/(2A^2n^4F^4C^2\sigma_w^2) \quad (2)$$

2.1.3 Thermogravimetric analysis

As shown in Fig.8, the weight loss before 500 ℃ is 1.35% and 20.09% for anatase and amorphous TiO_2 nanotubes, respectively. For the two samples, the weight loss can be attributed to the loss of adsorbed water. Thus, anatase TiO_2 nanotubes have a much lower amount of adsorbed water in comparison with amorphous TiO_2 nanotubes. The relatively low amount of physical adsorbed water on anatase TiO_2 nanotubes can be ascribed to post-heating at 500 ℃ for 4 h.

2.1.4 Morphological characterization after 100 discharge-charge cycles

Fig.9 presents the FESEM images of the electrodes after 100 discharge-charge cycles at 0.2C. Fig.9a and b show the morphology of anatase TiO_2 nanotube arrays after 100 cycles. A great number of nanotubular structures still can be observed. Although some of them are broken due to the strain produced in the discharge-charge process, the overall structure is well-retained without distinctive pulverization. These results reveal that anatase TiO_2 nanotubes are stable during the discharge-charge process. Fig.9c and d show the morphological characteristics of amorphous TiO_2 nanotube arrays after 100 cycles. In comparison with the results in Fig.2a, the original free-standing nanotube arrays have been severely damaged. Some wall fragments are observed, indicating that amorphous TiO_2 nanotubes are unstable during the discharge-charge process.

2.2 Discussion

For anatase TiO_2, it has long been investigated as the host structure for reversible lithium insertion and extraction. The crystalline structure of anatase is tetragonal (space group: $I4_1/amd$), which can be considered as a stacking of one-dimensional zigzag chains consisting of distorted edge-sharing TiO_6 octahedral [27]. This stacking leads to empty zigzag channels in the anatase framework, which facilitate diffusion of lithium ions in the anatase network. The electrochemical Li insertion/extraction reaction process can be described as Eq.3:

$$TiO_2 + xLi^+ + xe^- \longrightarrow Li_xTiO_2 \quad (3)$$

At x=0.5, a biphasic transition between tetragonal TiO_2 to orthorhombic $Li_{0.5}TiO_2$ occurs[27].

For anatase TiO_2 nanotube arrays, the discharge curves in Fig.3a can be divided into three different regions[28]: a monotonic voltage drop to 1.76 V is defined as the first region, in which homogeneous Li insertion up to the solid-solution limit of Li in TiO_2 occurs; the plateau at 1.76 V is the second region, which corresponds to the biphasic transition between tetragonal Li-poor phase to orthorhombic Li-rich phase and can be expressed by the Eq.**1**; after the plateau is the third region, and the contribution of Li storage can be ascribed to interfacial storage mechanism, which means the charge storage of lithium ions from faradic reactions occurring at the surface of TiO_2 nanotubes, referred to pseudocapacitive effect[25]. With the increase of surface area, the interfacial storage phenomenon becomes more pronounced [25]. As for amorphous TiO_2 nanotube arrays, the sloping discharge-charge curves in Fig.3b without a voltage plateau suggest that there is no a two-phase transition in amorphous TiO_2 nanotube array electrode during Li insertion/extraction process. Instead, Li storage results from a homogeneous Li insertion in TiO_2 solid solution and interfacial-based storage.

Even though the electrochemical results discussed above are consistent with the previous report, anatase TiO_2 nanotube arrays show a smaller width of the biphasic region and extension of lithium interfacial storage region compared with anatase TiO_2 nanotube arrays fabricated by anodization titanium in ionic liquid and post-heating [21]. This phenomenon indicates a more visible surface storage effect of anatase TiO_2 nanotube arrays fabricated by our method, suggesting their relatively large surface area to bulk ratio and thereby large proportion of surface and near-to-the surface atoms. In this work, anatase TiO_2 nanotubes have a wall thickness of only 30 nm and a mesoporous structure [16]. The contact area between electrolyte and electrode includes the out and inner surface of TiO_2 nanotube and

some exposed surface of the nanoparticles within the wall, which brings about a pronounced surface effect.

Besides, amorphous TiO_2 nanotube arrays exhibit a much larger initial irreversible discharge capacity than anatase TiO_2 nanotube arrays. It is explainable given the amount of adsorbed water and defects on the wall of TiO_2 nanotubes. TGA results above indicate amorphous TiO_2 nanotube arrays have a much larger amount of adsorbed water than anatase TiO_2 nanotube arrays. Water can react with Li^+ ion on the basis of Eq.**4**[14]:

$$H_2O+Li^++e^- \rightarrow LiOH+1/2H_2 \quad (\mathbf{4})$$

The irreversible consumption of lithium results in a much larger irreversible capacity of amorphous TiO_2 nanotube arrays. Thermal treatment at 500 ℃ for 4 h can effectively eliminate the adsorbed water, leading to relatively lower irreversible discharge capacity of anatase TiO_2 nanotube arrays.

In addition, amorphous TiO_2 nanotube arrays have much more structural and chemical defects, which also irreversibly consume lithium ions and lead to larger irreversible discharge capacity. Post-heating materials at higher temperature can greatly increase the crystallinity and reduce the defects. Thus, anatase TiO_2 nanotube arrays have a relatively low loss of the discharge capacity.

A superior rate capability of anatase TiO_2 nanotube arrays to amorphous electrode can be attributed to their lower charge-transfer resistance and higher lithium-ion diffusion coefficient revealed by EIS results. For amorphous TiO_2 nanotube arrays, there are a great number of defects, which produce many boundaries and thus hinder the electron transfer and the diffusion of lithium ions. Post-heating eliminates defects and improves the crystallization of TiO_2 nanotube arrays and thereby the kinetics of lithium ion intercalation and electron transfer.

An excellent cycling performance of anatase TiO_2 nanotube arrays can be ascribed to their stable crystal structure during the discharge-charge process. Amorphous TiO_2 nanotube arrays are fragile and cannot tolerate repeating discharge-charge process, thus breaking into fragments as observed in Fig.9c and d. Thermal treatment improves crystallization and mechanical strength of the tubular structure. Repeating insertion and extraction of lithium ions does not bring a great damage to the structure of anatase TiO_2 nanotubes, which can be verified by Fig.9a and b. Therefore, anatase TiO_2 nanotube arrays exhibit a superior cycling performance to amorphous TiO_2 nanotube arrays.

In comparison with other TiO_2 nanostructures, anatase TiO_2 nanotube arrays present an excellent electrochemical performance due to their one-dimensional nanotubular structure and direct contact with current collectors (copper substrates). These two advantages reduce the diffusion path of lithium ions and facilitate the electron transfer, thus leading to a superior electrochemical performance.

3 Conclusions

Lithium storage performances of amorphous and anatase TiO_2 nanotube arrays on copper substrate as electrodes in lithium-ion batteries have been respectively investigated. Free-standing amorphous TiO_2 nanotube arrays with lengths of 10~15 μm and diameters of 200~500 nm have been fabricated via a sacrificial template method based on outward coating of TiO_2 and inward etching of $Cu(OH)_2$ nanorod array templates on copper substrate. Anatase TiO_2 nanotube arrays can be prepared by post-heating the sample at 500 ℃ for 4 h. The lithium storage performances indicate that anatase TiO_2 nanotube arrays have a lower initial irreversible discharge capacity, better rate capability and capacity retention in comparison with amorphous TiO_2 nanotube arrays. The enhanced electrochemical performance of anatase TiO_2 nanotube arrays can be mainly ascribed to low amounts of adsorbed water, low charge-transfer resistance, high lithium-ion diffusion coefficient, high crystallization, and stable one-dimensional tubular structure on copper substrate.

Acknowledgements: This work is supported by the National Natural Science Foundation of China (NSFC Grants 21271058, 21176054, and 20871038) and the Education Department of Anhui Provincial Government (TD200702).

References:

[1] Wagemaker M, Kearley G J, Well A A, et al. *J. Am. Chem. Soc*., **2003**,**125**:840-848

[2] Macklin W J, Neat R J. *Solid State Ionics*, **1992**,**53**:694-700

[3] Chen J S, Lou X W. *Electrochem. Commun.*, **2009**,**11**:2332-2335

[4] Bao S J, Bao Q L, Li C M, et al. *Electrochem. Commun*., **2007**, **9**:1233-1238

[5] Xu J W, Jia C H, Cao B, et al. *Electrochim. Acta*, **2007**,**52**: 8044-8047

[6] Chen J S, Tan Y L, Li C M, et al. *J. Am. Chem. Soc*., **2010**, **132**:6124-6130

[7] Wang D W, Fang H T, Li F, et al. *Adv. Funct. Mater*., **2008**,**18**:3787-3793

[8] Jiang J, Liu J P, Ding R M, et al. *J. Phys. Chem. C*, **2010**,**114**: 929-932

[9] Wang J, Lin Z Q. *Chem. Mater*., **2008**,**20**:1257-1261

[10]Yoriya S, Paulose M, Varghese O K, et al. *J. Phys. Chem. C*, **2007**,**111**:13770-13776

[11]Lakshmi B B, Dorhout P K, Martin C R. *Chem. Mater.*, **1997**, **9**:857-862

[12]Li X H, Liu W M, Li H L. *Appl. Phys. A*, **2005**,**80**:317-320

[13]Tian Z R, Voigt J A, Liu J, et al. *J. Am. Chem. Soc*., **2003**, **125**:12384-12385

[14]Ortiz G F, Hanzu I, Djenizian T, et al. *Chem. Mater*., **2009**,**21**: 63-67

[15]Fang H T, Liu M, Wang D W, et al. *Nanotechnol.*, **2009**,**20**:1-7

[16]Zhang W X, Chen G D, Yang Z H, et al. *AIChE J.*, **2013**,**59**: 2134-2144

[17]Zhang W X, Xu J, Yang Z H, et al. *Chem. Phys. Lett*., **2007**, **434**:256-259

[18]Xu J, Zhang W X, Yang Z H, et al. *Inorg. Chem*., **2008**,**47**: 699-704

[19]Ortiz G F, Hanzu I, Knauth P, et al. *Electrochim. Acta*, **2009**, **54**:4262-4268

[20]Lou X W, Archer L A, Yang Z C. *Adv. Mater*., **2008**,**20**:3987-4019

[21]Li H Q, Martha S K, Unocic R R, et al. *J. Power Sources*, **2012**,**218**:88-92

[22]Pei B, Yao H X , Zhang W X, et al. *J. Power Sources*, **2012**, **220**:317-323

[23]Bard A J, Faulkner L R. *Electrochemical Methods*; Fundamentals and Applications. New York: John Wiley & Sons, Inc., **1980**:378-387

[24]Krol R, Goossens A, Schoonman J. *J. Phys. Chem. B*, **1999**, **103**:7151-7159

[25]Wang J, Polleux J, Lim J, et al. *J. Phys. Chem. C*, **2007**,**111**: 14925-14931.

[26]Cava R J, Murphy D W, Zahurak S. *J. Solid State Chem.*, **1984**,**53**:64-75

[27]Nuspl G, Yoshizawa K, Yamabe T. *J. Mater. Chem*., **1997**,**7**: 2529-2536

[28]Shin J Y, Samuelis D, Maier J. *Adv. Funct. Mater.*, **2011**,**21**: 3464-347